Title
Development of zirconium-89 PET for in vivo imaging of alpha-klotho.

Journal
Am j nucl med mol imaging, 10(2)

ISSN
2160-8407

Authors
Lau, Wei Ling
Liang, Christopher
Liu, Han
et al.

Publication Date
2020

Peer reviewed

Am J Nucl Med Mol Imaging 2020;10(2):95-105
www.ajnmmi.us /ISSN:2160-8407/ajnmmi0110442

Original Article

Development of zirconium-89 PET for *in vivo* imaging of alpha-klotho

Wei Ling Lau[1*], Christopher Liang[2*], Han Liu[1], Karanveer Singh[2], Jogeshwar Mukherjee[2]

[1]Nephrology, Department of Medicine, University of California-Irvine, Irvine, CA 92697, USA; [2]Preclinical Imaging, Radiological Sciences, University of California-Irvine, Irvine, CA 92697, USA. [*]Equal contributors.

Received February 4, 2020; Accepted March 24, 2020; Epub April 15, 2020; Published April 30, 2020

Abstract: Alpha-klotho is a single-pass membrane protein primarily expressed by the kidneys. Klotho deficiency in chronic kidney disease contributes to an accelerated aging phenotype. We report here development of [^{89}Zr]DFO-anti-klotho positron emission tomography (PET) imaging as a novel non-invasive method for assessing whole-body alpha-klotho distribution. Rat monoclonal anti-mouse klotho antibody was reacted with SCN-Bn-deferoxamine (DFO) and was radiolabeled using Zirconium-89. *In vitro* testing of [^{89}Zr]DFO-anti-mKlotho was done in a distal convoluted tubule kidney cell line and with 40-micron whole kidney sections from C57BL/6J mice. Competitive binding was assessed in co-incubation studies with unlabeled anti-mKlotho antibody. For *in vivo* testing, C57BL/6J mice were injected retro-orbitally with [^{89}Zr]DFO-anti-mKlotho and were scanned using Inveon PET/CT. Autoradiographs of kidney sections were obtained post-imaging on select animals. Radiochemical yield of [^{89}Zr]DFO-anti-mKlotho was >70% and radiochemical purity was confirmed by iTLC. Specific binding in the kidney cell line was reduced by 60% in the presence of unlabeled anti-mKlotho. In the PET/CT scans, initial uptake of [^{89}Zr]DFO-anti-mKlotho was observed in the intestines and liver. Selective retention of radioactivity was observed in the kidneys in the subsequent 24, 48, and 72 hrs scans with cortical binding of [^{89}Zr]DFO-anti-mKlotho clearly visualized. Sites of lower alpha-klotho expression were not visualized. In summary, we have successfully synthesized [^{89}Zr]DFO-anti-mKlotho and our initial *in vitro* and *in vivo* studies in mice demonstrate selective binding in the kidney cortex, which is known to express high levels of alpha-klotho. PET imaging promises to be a novel tool for *in vivo* evaluation of alpha-klotho distribution.

Keywords: [^{89}Zr]DFO-anti-mKlotho, alpha-klotho, monoclonal antibodies, autoradiography, PET/CT imaging

Introduction

Alpha-klotho was first discovered in 1997 [1] and was named after the Greek goddess Clotho who spins the thread of life because of the molecule's important role in regulating metabolism and longevity. Alpha- and beta-klotho may play a crucial role in the pathophysiology of aging-related disorders such as diabetes, cancer, arteriosclerosis, and chronic kidney disease [2]. Alpha-klotho is a 130 kDa transmembrane protein with 80% homology between rodents and humans, and functions as the co-receptor for fibroblast growth factor-23 (FGF23) to facilitate FGF23 binding to FGF receptors. FGF23-klotho signaling induces kidney phosphorus excretion and inhibits activity of vitamin D 1α-hydroxylase. A decrease in alpha-klotho is associated with infertility, secondary hyperthyroidism, vascular calcification, cardiac hypertrophy, progression of chronic kidney disease, skin atrophy and osteoporosis [1, 3].

Expression of alpha-klotho is primarily in the distal convoluted tubules of the kidney cortex [4]. Low-level expression of alpha-klotho is present in the choroid plexus of the brain and the parathyroid gland. There is controversy surrounding tissue expression of alpha-klotho with discrepancies between animal and human studies, especially in regard to the cardiovascular system [4-6]. Non-invasive methods to examine tissue distribution of alpha-klotho protein *in vivo* are currently lacking; we propose that development of alpha-klotho imaging would facilitate ongoing research exploring induction of alpha-klotho as a therapeutic target in aging and kidney disease (e.g., novel small chemical compounds and pharmaceutical agents such as active vitamin D and peroxi-

some proliferator-activated receptor-γ (PPARγ) [2, 7]).

Our goal for this project was to develop a positron emission tomography (PET) imaging tool to facilitate *in vivo* detection of alpha-klotho. Zirconium-89 (^{89}Zr) was chosen as a suitable radioisotope for this study since it possesses a long half-life and has been extensively studied for radiolabeled antibody imaging studies in humans, primary in oncology. For example, ^{89}Zr-labeled antibodies have been used in high-resolution targeted PET-computed tomography (PET/CT) detection of breast cancer [8-12], multiple myeloma cell imaging [13], ovarian cancer [14-17], prostate cancer [18-20], renal and squamous cell carcinoma [21-25] and colon cancer [26-28]. We applied published methods to develop ^{89}Zr radiolabeling of rat monoclonal anti-mouse klotho antibody and herein describe *in vitro* characterization of the ^{89}Zr-mKlotho conjugate as well as *in vivo* PET/CT scans in live C57BL/6J mice.

Materials and methods

General methods

All commercially available reagents and solvents were purchased from Sigma-Aldrich (St. Louis, MO) unless specified and used without any further purification. p-SCN-Deferoxamine was purchased from Macrocyclics (Plano, TX). Zr-89 in 1 M oxalic acid was produced by 3D Imaging LLC (Little Rock, AR). Rat anti-mouse klotho monoclonal antibody MAB1819 was purchased from R&D Systems (Minneapolis, MN). Water was purified using a MilliQ filtration system. Bio-Rad 6 spin columns were purchased from Bio-Rad (Hercules, CA). PD-10 filtration columns were purchased from GE Healthcare (Chicago, IL). Mass spectrometry was performed using a ESI LC-ToF Micromass LCT Premier (Waters Co., Milford, MA) and Xevo G2-XS ToF-MS (Waters). Analysis of mass spectrometry results was done using MassLynx 4.0 (Waters). Instant thin layer chromatography (iTLC) was performed using chromatography stripes purchased from Biodex and scanned on an AR-2000 Radio-TLC Imaging Scanner (Eckart & Ziegler, Berlin, Germany). Mouse kidney slices were obtained on a Leica 1850 cryotome. Zirconium-89 autoradiographic studies were carried out by exposing tissue samples on storage phosphor screens (Multisensitive Medium MS, PerkinElmer, Waltham, MA). The apposed phosphor screens were read and analyzed by OptiQuant acquisition and the Cyclone Storage Phosphor System (Packard Instruments Co., Boston, MA). A preclinical Inveon dedicated PET scanner (Siemens Medical Solutions, Knoxville, TN) with a transaxial FWHM of 1.46 mm, and axial FWHM of 1.15 mm [29] was used for the PET studies. PET/CT images of mice were obtained and analyzed using ASIProVM and IRW software platforms (Siemens). All animal studies were approved by the Institutional Animal Care and Use Committee of University of California-Irvine.

Synthesis of DFO-anti-mKlotho

The synthesis and radiolabeling of our compound was adapted from a previously published protocol [30]. Anti-mKlotho antibody (500 μg) was dissolved in 0.5 mL sterile saline to create a 0.5 mg/0.5 mL solution of antibody. 450 μL of the resulting solution was added to an Eppendorf tube and 0.1 mL of 0.48 M Na_2CO_3 was added to raise the solution pH to 9. The solution was vortexed briefly and allowed to rest for 5 minutes. 9 mg DFO was dissolved in 1 mL DMSO; purity of the DFO was confirmed using mass spectrometry. 20 μL of the DFO solution was added to the anti-mKlotho antibody solution in 5 μL aliquots. The mixture was incubated at 37°C for 30 minutes while being gently shaken (**Figure 1**). The solution was loaded in 100 μL batches into 6 Bio-Rad 6 spin columns and centrifugation was done, discarding the elution. Following first centrifugation, 100 μL saline was added to each Bio-Rad 6 spin column and DFO-anti-mKlotho product was collected in the second elution.

To confirm successful synthesis of DFO-anti-mKlotho, a 20 μg sample was first treated with dithiothreitol (DTT) to expose the fragments of the antibody. The sample was then analyzed alongside of a pure sample of unconjugated anti-mKlotho antibody using a Xevo G2-XS ToF-MS. DTT-treated pure mKlotho antibody yielded a weight of 24,085 daltons for the klotho fragment. DTT-treated DFO-mKlotho showed both an unlabeled klotho fragment (24,085 daltons) as well as a modified DFO-mKlotho fragment, which was 24,837 daltons (**Figure 2**). Since the weight of DFO is 752 and 24,085+752 = 24,837, we thus confirmed that our reaction

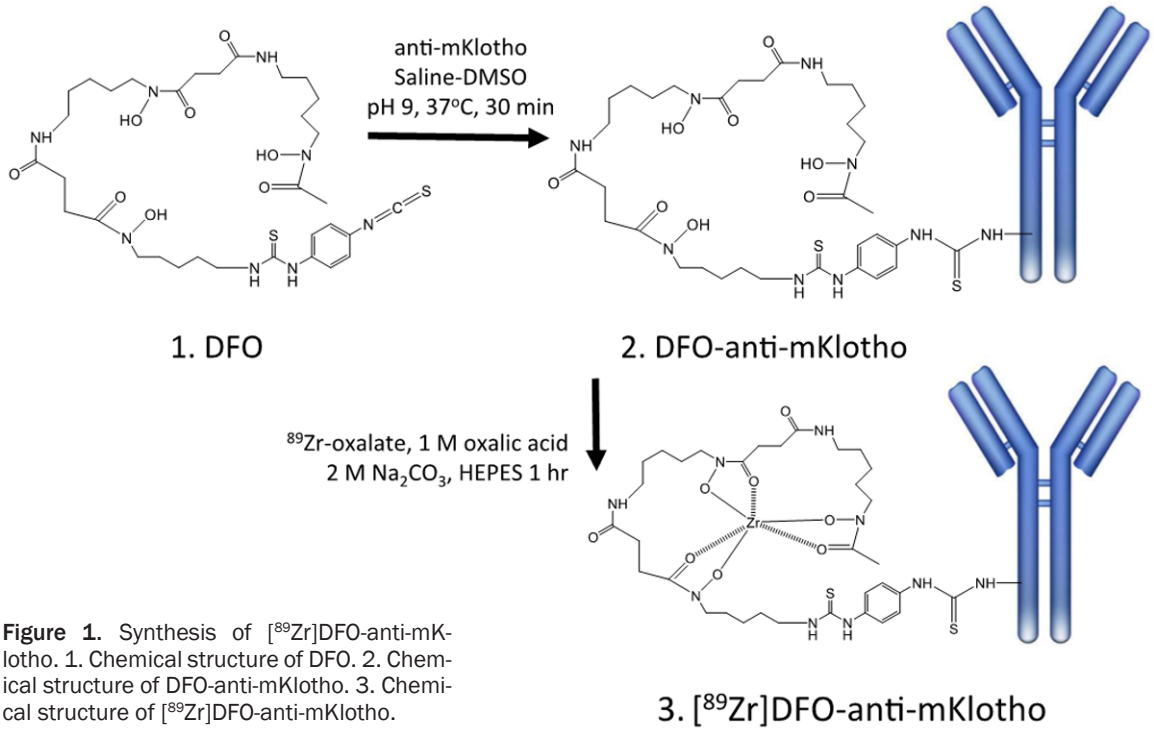

Figure 1. Synthesis of [^{89}Zr]DFO-anti-mKlotho. 1. Chemical structure of DFO. 2. Chemical structure of DFO-anti-mKlotho. 3. Chemical structure of [^{89}Zr]DFO-anti-mKlotho.

was successful and we had modified the mKlotho antibody with the chelator DFO.

Radiosynthesis of [^{89}Zr]DFO-anti-mKlotho

92.13 MBq of [^{89}Zr]oxalate was added to a reaction vial containing 200 µL 1 M oxalic acid. 90 µL of 2 M Na_2CO_3 was then added and the reaction mixture was allowed to sit for 3 min. HEPES buffer (pH 7.1-7.3; 0.7 mL) was then added followed by the pooled DFO-anti-mKlotho product. The mixture was incubated for one hour at R.T. with gentle shaking (**Figure 1**).

Afterward, the mixture was purified on a PD-10 column that had been prewashed with gentisic acid (5 mg/mL in 0.25 M NaOAc) and eluted using gentisic acid to collect [^{89}Zr]DFO-anti-mKlotho. A 1.5 mL waste fraction was discarded before collecting the first 2 mL fraction. Afterward, nine more 1 mL fractions were eluted from the PD-10 column. The fractions with the highest radioactivity counts were used for *in vivo* experiments. To confirm successful radiolabeling of DFO-anti-mKlotho with ^{89}Zr, a sample from one of the selected fractions was used to dot an iTLC chromatography strip that was developed and scanned on a AR-2000 Radio-TLC Imaging Scanner (Eckart & Ziegler). Apparent specific activity of [^{89}Zr]DFO-anti-mKlotho was calculated to be around 0.185 MBq/µg.

In vitro binding assays

In vitro testing of [^{89}Zr]DFO-anti-mKlotho was done with kidney cell lines and 40-micron cryotome sections of mouse whole kidney. Competitive binding was assessed using unlabeled anti-mKlotho antibody. Kidney distal convoluted cells (catalog# ATCC CRL-3250, American Type Culture Collection, Manassas, VA) were expanded and 12 microfuge tubes containing 6.8 million cells each were incubated with 703 MBq [^{89}Zr]DFO-anti-mKlotho per tube. For non-specific binding, anti-mKlotho was also added to 6 of the tubes (5 µg/mL); final volume was 0.5 mL per sample. Following a 1 hour incubation, the samples were filtered and the microfuge tubes were exposed on phosphor screens.

In vivo mouse PET/CT imaging

Adult male and female C57BL/6J mice were obtained from Jackson Laboratory (Bar Harbor, ME). Under isoflurane anesthesia, [^{89}Zr]DFO-anti-mKlotho 0.925-1.369 MBq was given in-

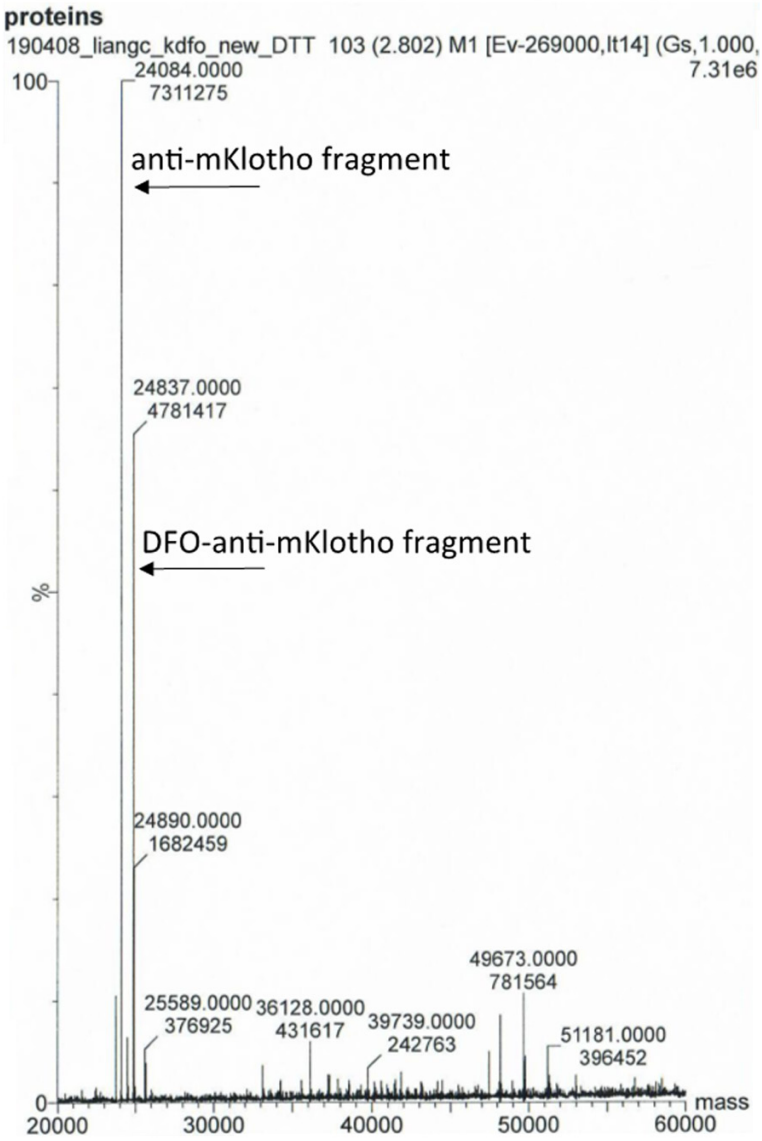

Figure 2. Characterization of DFO-mKlotho fragment on mass spectrometry. DTT-treated pure mKlotho antibody yielded a weight of 24,085 daltons for the klotho fragment. DTT-treated DFO-mKlotho showed both an unlabeled klotho fragment (24,085 daltons) as well as a modified DFO-mKlotho fragment, which was 24,837 daltons. Since the weight of DFO is 752 and 24,085+752 = 24,837, we thus confirmed that our reaction was successful and we had modified the mKlotho antibody with the chelator DFO.

travenously via retro-orbital injection. A blocking study was attempted using 10 mg of unlabeled anti-mKlotho that was injected 1 hour prior to the [^{89}Zr]DFO-anti-mKlotho dose.

Scanning was done on the mice at 2, 24, 48 and 72 hr after injection of [^{89}Zr]DFO-anti-mKlotho. The mice were anesthetized using 4% isoflurane gas and then positioned in the mouse chamber of the Inveon Multimodality CT/PET scanner. Anesthesia was maintained with 2-2.5% isoflurane during the scans. Whole body scans were performed using Inveon Multimodality (MM) CT scanner and Inveon Dedicated PET scanner (Siemens). CT images of the mice were obtained with a large area detector (4096 × 4096 pixels, 10 cm × 10 cm field-of-view). The CT projections were acquired with the detector-source assembly rotating over 360 degrees and 720 rotation steps. The mice underwent a single-bed low resolution CT scan at 80 kV/500 uA and a 30-minute PET scan under isoflurane anesthesia for a total scan time of 35-40 min. PET images were reconstructed using the OSEM3D protocol.

Ex vivo studies

After the PET/CT scan, the mice under anesthesia were sacrificed by cardiac exanguination and the kidneys were rapidly removed and frozen in dry ice. Kidney sections of 40-micron thickness were generated on a cryotome and mounted on glass slides. The slides were then exposed on storage phosphor screens and analyzed.

Image analysis

The scans were analyzed using Inveon Research Workplace. Regions of interest (ROIs) were first determined by looking at the CT scan and locating the kidneys. Separate ROIs were drawn around the kidney cortex and medulla with care taken to avoid overlap of the two ROIs. ROIs were constructed to be approximately the same size. The mean uptake of the respective regions was recorded in Bq/mL. Standardized uptake values (SUVs) were calculated using recorded weights and injection doses. Screenshots were obtained using the in-program screenshot option. 3D images were generated using the

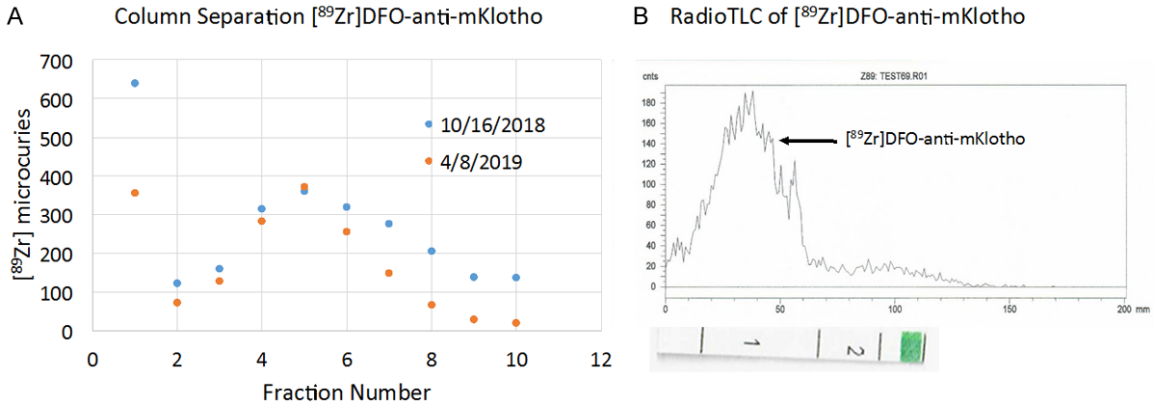

Figure 3. Radiosynthesis results and purity analysis. A. The amount of [^{89}Zr]DFO-anti-mKlotho activity obtained in each fraction of the PD-10 elution. B. RadioTLC of the completed product confirming that the majority of the eluted product stays within region 1 of the iTLC strip, consistent with successful radiolabeling.

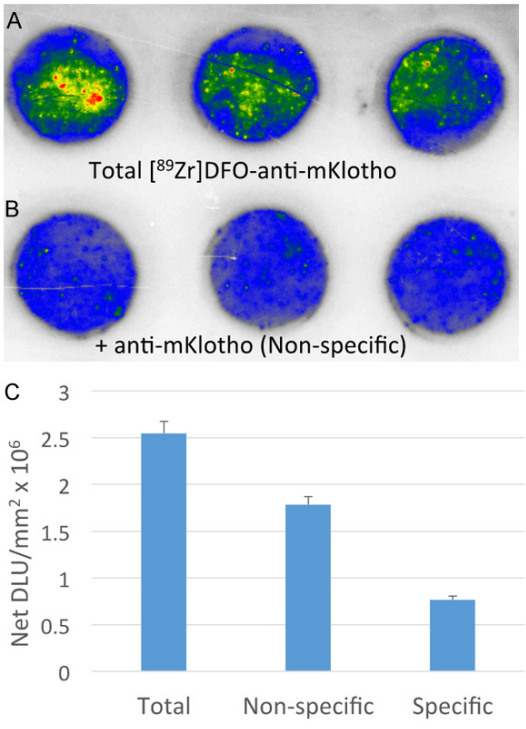

Figure 4. Autoradiograph of distal convoluted tubule kidney cell line featuring total binding and non-specific binding. A. Total binding of [^{89}Zr]DFO-anti-mKlotho. B. Non-specific binding measured in the presence of 5 mg/mL of anti-mKlotho. C. The chart summarizes radioactive uptake (digital light units, DLU/mm^2) of the [^{89}Zr]DFO-anti-mKlotho with calculated total, non-specific and specific binding values. The specific binding of [^{89}Zr]DFO-anti-mKlotho in the cultured kidney cell line, derived from blocking studies with unlabeled anti-mKlotho antibody, was 30-40%.

Inveon Research Workplace 3D Visualization program.

Results

Synthesis of DFO-anti-mKlotho

We achieved successful synthesis of DFO-anti-mKlotho consistent with previously reported methods [30] (**Figure 1**). We did require one modification whereby the spin columns had to be centrifuged twice in order to elute the DFO-anti-mKlotho product. It remains unclear why the elution rate was slower compared to published methods, however mass spectrometry confirmed successful synthesis of DFO-anti-mKlotho despite the delayed elution time.

Radiosynthesis of [^{89}Zr]DFO-anti-mKlotho

Synthesis of [^{89}Zr]DFO-anti-mKlotho was successfully carried out published Zr-89 methods [30] with a radiochemical yield of greater than 70%. The majority of the [^{89}Zr]DFO-anti-mKlotho eluted within 6-8 fractions (**Figure 3A**). RadioTLC determined that radiochemical purity was greater than 90%; aqueous citrate eluent, Rf<0.1 (**Figure 3B**). Apparent specific activity of [^{89}Zr]DFO-anti-mKlotho was calculated to be approximately 0.185 MBq/μg.

In vitro binding affinity studies

As expected, [^{89}Zr]DFO-anti-mKlotho showed significant binding to cultured distal convoluted tubule kidney cells which are known to express alpha-klotho [4]. In the presence of unlabeled anti-mKlotho antibody, specific binding was reduced by 60% with signal from the radiolabeled compound reduced to 30-40% (**Figure 4**).

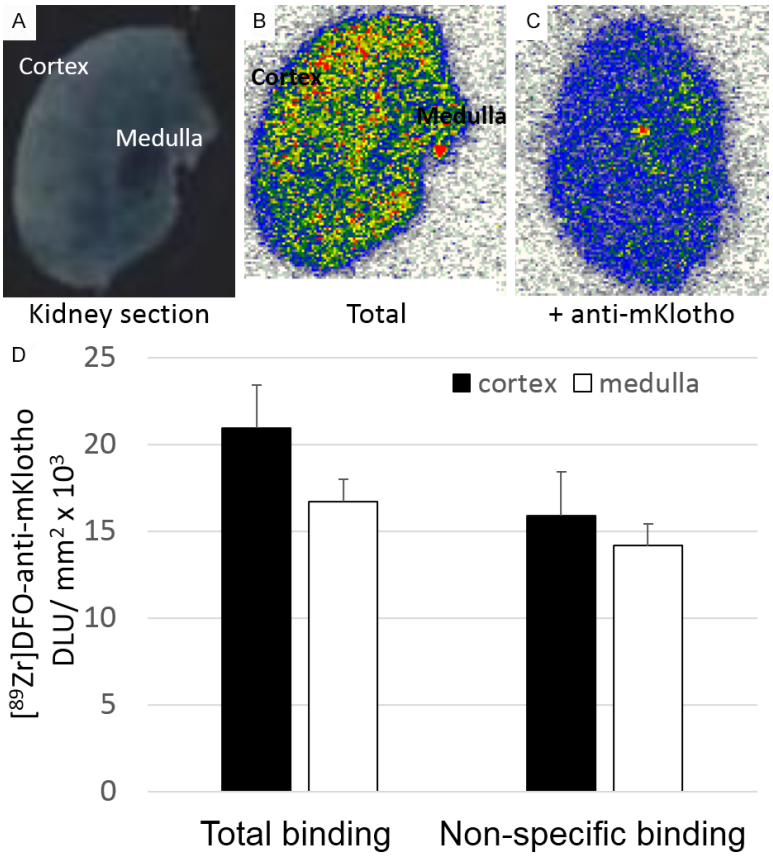

Figure 5. *In vitro* [^{89}Zr]DFO-anti-mKlotho binding in kidney sections. (A) Cryopreserved mouse kidney sections (40-micron thickness) were incubated with [^{89}Zr]DFO-anti-mKlotho. (B) Total binding of [^{89}Zr]DFO-anti-mKlotho. (C) Non-specific binding where sections were pre-incubated with unlabeled anti-mKlotho (1.5 mg/ml). (D) Plot showing total and nonspecific binding of [^{89}Zr]DFO-anti-mKlotho in (B and C). There was greater binding within the cortex compared to the medulla with a ratio of 1.25. Ratio of total cortex to nonspecific cortex was 1.32.

In vitro incubation with the cryo-preserved kidney sections showed that the majority of [^{89}Zr]DFO-anti-mKlotho binding was within the kidney cortex with lesser binding detected in the medulla (**Figure 5**). The ratio of cortex:medulla signal was calculated at 1.25. When co-incubated with unlabeled anti-mKlotho antibody, nonspecific binding was high indicating successful blocking of alpha-klotho antigen sites.

In vivo PET/CT scans

Two male and 5 female mice completed *in vivo* imaging. Due to initial difficulties with tracer injections leading to poor tissue signal, we had limited imaging data from male animals. PET/CT scans showed initial uptake of [^{89}Zr]DFO-anti-mKlotho in the intestines and liver, followed by persistent distinct binding of [^{89}Zr]DFO-anti-mKlotho in the kidneys within 24 hours of injection. Localization of binding was confirmed using the co-registered CT scan. The majority of [^{89}Zr]DFO-anti-mKlotho signal was in the kidney cortex, with lower intensity in the kidney medulla (**Figure 6**). Serial PET/CT scans showed mild decrease in [^{89}Zr]DFO-anti-mKlotho activity within the kidneys due to radioactive decay at 48 and 72 hours after injection. Binding was symmetric in both kidneys and the ratio of cortex:medulla uptake was 1.32. The liver had detectable but much lower uptake of the radiolabeled antibody. The PET scans did not demonstrate [^{89}Zr]DFO-anti-mKlotho binding in other organs. In one mouse with 10 μg unlabeled anti-mKlotho antibody injected 1 hour prior to [^{89}Zr]DFO-anti-mKlotho (blocking study), no significant reduction in the binding of [^{89}Zr]DFO-anti-mKlotho was observed. This may be due to the low dose of unlabeled anti-mKlotho antibody (limited by cost) and/or a general difficulty in carrying out displacement/blocking studies with antibodies.

Ex vivo studies

Kidneys were harvested 72 hours after retro-orbital injection of [^{89}Zr]DFO-anti-mKlotho, following completion of PET/CT scans. Cryopreserved *ex vivo* kidney sections exposed on phosphor screens demonstrated localized binding in the kidney cortex with minimal uptake in the medulla (**Figure 7**). The ratio of uptake in the cortex versus medulla in the female mouse was 3.74 versus a lower cortex:medulla ratio of 2.72 in the male mouse.

Discussion

In vivo intravenous administration of [^{89}Zr]DFO-anti-mKlotho demonstrated localized binding in the kidneys, consistent with the kidneys being the primary source of alpha-klotho. There was higher binding in the cortex than the medulla of

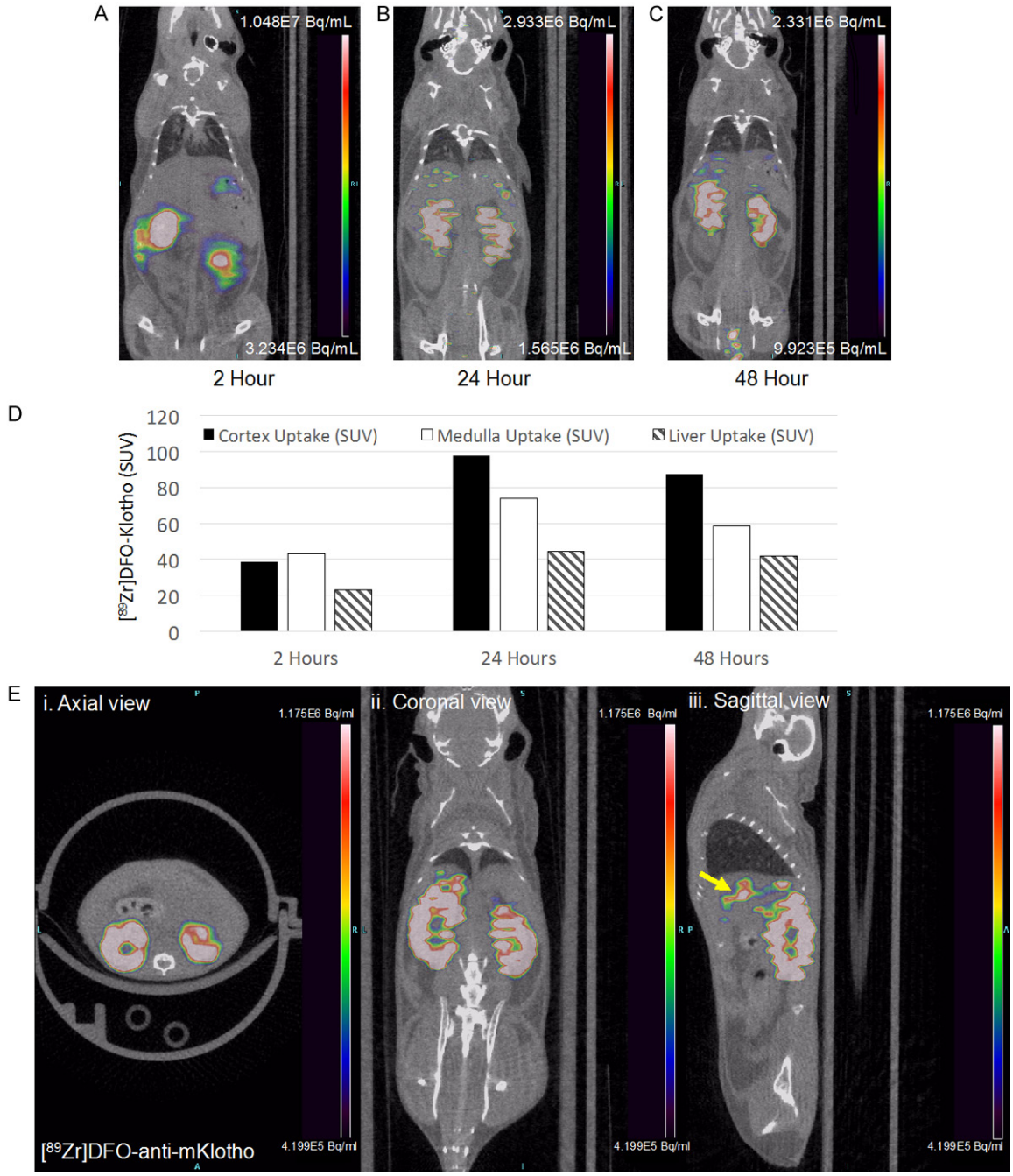

Figure 6. Sequential 30-minute static scans of [^{89}Zr]DFO-anti-mKlotho distribution. PET/CT imaging was done at (A) 2 hours, (B) 24 hours, and (C) 48 hours after retro-orbital injection of [^{89}Zr]DFO-anti-mKlotho. (D) Standardized uptake values (SUVs) summarized in the graph show optimal uptake of the radiolabeled antibody in the kidneys at 24 hours, with slight decay of radioactivity after 48 hours. The ratio of cortex:medulla signal was 1.32 at 24 hours and 1.49 at 48 hours. (E) Axial (left panel), coronal (middle panel) and sagittal (right panel) images taken 72 hours after injection of [^{89}Zr]DFO-anti-mKlotho in a female mouse, demonstrating persistent strong radioactivity in the kidneys. A region of activity in the liver was also noted (yellow arrow).

the kidneys and this signal was attenuated in blocking studies with unlabeled anti-mKlotho antibody. *In vitro* binding with a distal convoluted tubule cell line and kidney sections showed similar results with blocking of [^{89}Zr]DFO-anti-mKlotho by unlabeled antibody; however *in vitro* studies were limited by low specific binding.

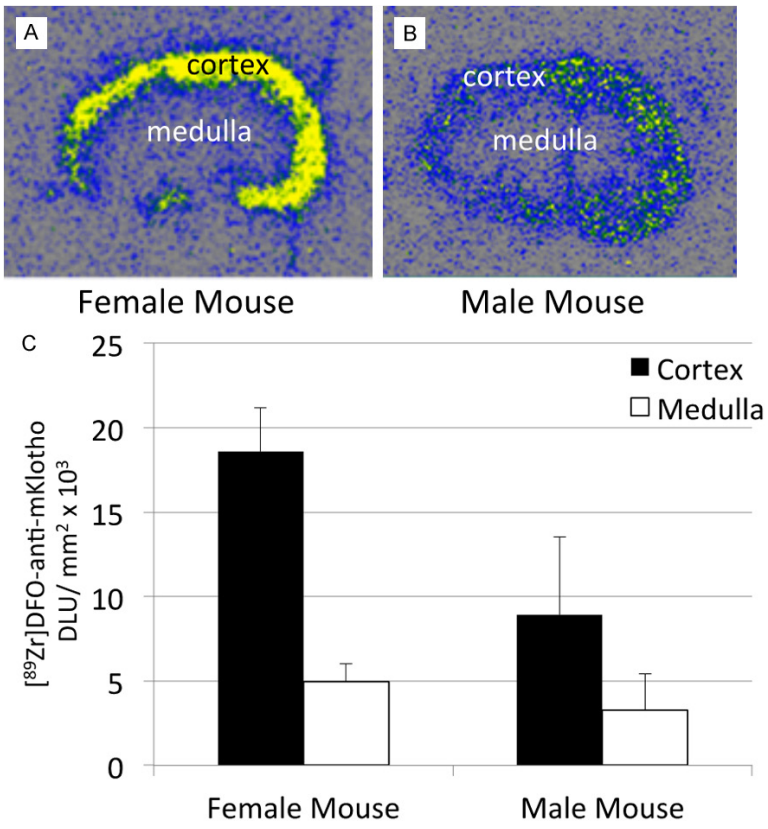

Figure 7. *Ex vivo* images of kidney sections harvested from mice after PET/CT imaging. Imaging of the kidneys harvested from mice 72 hours after retro-orbital injection of [^{89}Zr]DFO-anti-mKlotho showed more robust cortex:medulla selective activity than the *in vitro* studies. A. Female mouse kidney section showing distinct binding in the cortex. B. Male mouse kidney section showing lower binding in the cortex compared to the female. C. Plot shows results from A and B cortex and medulla binding of [^{89}Zr]DFO-anti-mKlotho. The ratio of kidney cortex binding compared to medulla was 2.72 in male animals and 3.74 in female animals.

The discrepancy between the strong *in vivo* PET/CT kidney cortex signal (confirmed on *ex vivo* kidney sections) and the low *in vitro* specific binding (in cultured cells and kidney sections) is likely due to alpha-klotho trafficking across renal tubules that happens *in vivo*. Hu et al. previously demonstrated that transcytosis of alpha-klotho from the blood circulation occurs from basolateral to intracellular location, with subsequent secretion across the apical membrane in both proximal and distal tubules [31]. The selective targeting of the kidneys by labeled [^{89}Zr]DFO-anti-mKlotho that was persistent out to 72 hours post-injection was unlikely to be due to nonspecific glomerular filtration, since previous studies reported that [^{89}Zr]DFO clears out quickly from the urinary system within an hour after injection and shows only minimal retention in the kidneys [30, 32]. There was little background noise in the PET scans outside of the liver, which had marginal uptake of the antibody. This could be due to continued processing of [^{89}Zr]DFO-anti-mKlotho through the bloodstream, as there is no reported literature of [^{89}Zr]DFO being trapped within the liver.

We were able to detect localization of ^{89}Zr-labeled alpha-Klotho antibody in the kidney, which is likely to have concentrations greater than 500 pg/ml based on extrapolation from serum alpha-klotho data [2]. While prior *in vitro* investigations have shown that there are alpha-klotho production sites within the choroid plexus and the parathyroid gland [4], there was no discernible [^{89}Zr]DFO-anti-mKlotho binding to these sites *in vivo* in the current study. This may be due to the blood-brain barrier being impermeable to the complexed agent, preventing access to the choroid plexus. With regard to the parathyroid gland, it is possible that [^{89}Zr]DFO-anti-mKlotho concentration *in vivo* was not high enough to produce a detectable signal. Further, it has been proposed that extra-renal alpha-klotho production may be low or undetectable under normal alpha-klotho status in the setting of intact kidney function [31].

The *ev vivo* results with the kidney slices showed a significant difference in uptake between the kidney cortex and the kidney medulla, with 2.7-3.7 times higher uptake in the cortex than medulla (**Figure 7**). These results are the most significant finding to come out of our experiments, since the kidney cortex is the major source of alpha-klotho production within the body. Female mice showed more robust cortex:medulla binding than male animals; the physiologic relevance of this is unclear at this

time. Sex- and age-dependent modulation of alpha-klotho has been reported in humans; serum alpha-klotho levels are higher in young girls compared to boys, whereas cerebrospinal fluid alpha-klotho is lower in females in the geriatric population [33, 34].

In summary, [^{89}Zr]DFO-anti-mKlotho is a novel radiolabeled antibody that can be used for selective imaging of alpha-klotho protein *in vivo*. The synthesis protocol resulted in high radiochemical purity and yield. There is little degradation of the DFO complex *in vivo*, providing a clear picture of the compound's biodistribution. The radiolabeled antibody travels selectively to the kidneys, with minor binding located in the liver. *In vivo* scans and *ex vivo* autoradiographs show intense uptake within the kidney cortex compared to the medulla, which is consistent with previous *in vitro* studies of alpha-klotho. In future studies we plan to utilize [^{89}Zr] DFO-anti-mKlotho PET/CT imaging to examine alpha-klotho biodistribution in models of alpha-klotho deficiency such as chronic kidney disease and aging.

Acknowledgements

This work was supported by an American Heart Association Innovative Research Grant 17IRG-33410803 (WLL). We thank the UCI Undergraduate Research Opportunities Program for support (KS), and acknowledge valuable input from Anna Wu (Radiation Oncology, City of Hope, Los Angeles, CA), Felix Bergara (Molecular and Medical Pharmacology University of California-Los Angeles), Ming Chang Hu and Orson Moe (Nephrology/Internal Medicine, UT Southwestern, Dallas, TX) during the design of the experiments. Pilot findings from this project were presented in an oral abstract at the 2019 Society of Nuclear Medicine and Molecular Imaging (SNMMI) Annual Meeting (Anaheim, CA, June 2019).

Disclosure of conflict of interest

None.

Address correspondence to: Dr. Wei Ling Lau, Division of Nephrology & Hypertension, University of California Irvine, 101 The City Drive South, City Tower, Suite 400, Irvine, CA 92697, USA. Tel: 714-456-5142; Fax: 714-456-6034; E-mail: wllau@uci.edu

References

[1] Kuro-o M, Matsumura Y, Aizawa H, Kawaguchi H, Suga T, Utsugi T, Ohyama Y, Kurabayashi M, Kaname T, Kume E, Iwasaki H, Iida A, Shiraki-Iida T, Nishikawa S, Nagai R and Nabeshima YI. Mutation of the mouse klotho gene leads to a syndrome resembling ageing. Nature 1997; 390: 45-51.

[2] Kuro-O M. The Klotho proteins in health and disease. Nat Rev Nephrol 2019; 15: 27-44.

[3] Hu MC, Shiizaki K, Kuro-o M and Moe OW. Fibroblast growth factor 23 and Klotho: physiology and pathophysiology of an endocrine network of mineral metabolism. Annu Rev Physiol 2013; 75: 503-33.

[4] Olauson H, Mencke R, Hillebrands JL and Larsson TE. Tissue expression and source of circulating αKlotho. Bone 2017; 100: 19-35.

[5] Lim K, Groen A, Molostvov G, Lu T, Lilley KS, Snead D, James S, Wilkinson IB, Ting S, Hsiao LL, Hiemstra TF and Zehnder D. α-Klotho expression in human tissues. J Clin Endocrinol Metab 2015; 100: E1308-E1318.

[6] Mencke R, Harms G, Mirković K, Struik J, Van Ark J, Van Loon E, Verkaik M, De Borst MH, Zeebregts CJ, Hoenderop JG, Vervloet MG, Hillebrands JL and Consortium N. Membrane-bound Klotho is not expressed endogenously in healthy or uraemic human vascular tissue. Cardiovasc Res 2015; 108: 220-231.

[7] Jung D, Xu Y and Sun Z. Induction of anti-aging gene klotho with a small chemical compound that demethylates CpG islands. Oncotarget 2017; 8: 46745-46755.

[8] Stergiou N, Nagel J, Pektor S, Heimes AS, Jäkel J, Brenner W, Schmidt M, Miederer M, Kunz H, Roesch F and Schmitt E. Evaluation of a novel monoclonal antibody against tumor-associated MUC1 for diagnosis and prognosis of breast cancer. Int J Med Sci 2019; 16: 1188-1198.

[9] Dijkers EC, Oude Munnink TH, Kosterink JG, Brouwers AH, Jager PL, de Jong JR, van Dongen GA, Schröder CP, Lub-de Hooge MN and de Vries EG. Biodistribution of 89Zr-trastuzumab and PET imaging of HER2-positive lesions in patients with metastatic breast cancer. Clin Pharmacol Ther 2010; 87: 586-92.

[10] Hong H, Severin GW, Yang Y, Engle JW, Zhang Y, Barnhart TE, Liu G, Leigh BR, Nickles RJ and Cai W. Positron emission tomography imaging of CD105 expression with 89Zr-Df-TRC105. Eur J Nucl Med Mol Imaging 2012; 39: 138-148.

[11] Jacobson O, Zhu L, Niu G, Weiss ID, Szajek LP, Ma Y, Sun X, Yan Y, Kiesewetter DO, Liu S and Chen X. MicroPET imaging of integrin αvβ3 expressing tumors using 89Zr-RGD peptides. Mol Imaging Biol 2011; 13: 1224-1233.

[12] Heskamp S, van Laarhoven HWM, Molkenboer-Kuenen JD, Franssen GM, Versleijen-Jonkers YM, Oyen WJ, van der Graaf WT and Boerman OC. ImmunoSPECT and immunoPET of IGF-1R expression with the radiolabeled antibody R1507 in a triple-negative breast cancer model. J Nucl Med 2010; 51: 1565-72.

[13] Ghai A, Maji D, Cho N, Chanswangphuwana C, Rettig M, Shen D, DiPersio J, Akers W, Dehdashti F, Achilefu S, Vij R and Shokeen M. Preclinical development of CD38-targeted [89Zr]Zr-DFO-daratumumab for imaging multiple myeloma. J Nucl Med 2018; 59: 216-222.

[14] Meijs WE, Haisma HJ, Klok RP, van Gog FB, Kievit E, Pinedo HM and Herscheid JD. Zirconium-labeled monoclonal antibodies and their distribution in tumor-bearing nude mice. J Nucl Med 1997; 38: 112-8.

[15] Nagengast WB, Lub-de Hooge MN, Oosting SF, den Dunnen WF, Warnders FJ, Brouwers AH, de Jong JR, Price PM, Hollema H, Hospers GA, Elsinga PH, Hesselink JW, Gietema JA and de Vries EG. VEGF-PET imaging is a noninvasive biomarker showing differential changes in the tumor during sunitinib treatment. Cancer Res 2011; 71: 143-53.

[16] Nagengast WB, de Vries EG, Hospers GA, Mulder NH, de Jong JR, Hollema H, Brouwers AH, van Dongen GA, Perk LR and Lub-de Hooge MN. In vivo VEGF imaging with radiolabeled bevacizumab in a human ovarian tumor xenograft. J Nucl Med 2007; 48: 1313-9.

[17] Terwisscha van Scheltinga AG, van Dam GM, Nagengast WB, Ntziachristos V, Hollema H, Herek JL, Schröder CP, Kosterink JG, Lub-de Hoog MN and de Vries EG. Intraoperative near-infrared fluorescence tumor imaging with vascular endothelial growth factor and human epidermal growth factor receptor 2 targeting antibodies. J Nucl Med 2011; 52: 1778-1785.

[18] Holland JP, Divilov V, Bander NH, Smith-Jones PM, Larson SM and Lewis JS. 89Zr-DFO-J591 for immunoPET of prostate-specific membrane antigen expression in vivo. J Nucl Med 2010; 51: 1293-1300.

[19] Ruggiero A, Holland JP, Hudolin T, Shenker L, Koulova A, Bander NH, Lewis JS and Grimm J. Targeting the internal epitope of prostate-specific membrane antigen with 89Zr-7E11 immuno-PET. J Nucl Med 2011; 52: 1608-15.

[20] van Rij CM, Sharkey RM, Goldenberg DM, Frielink C, Molkenboer JD, Franssen GM, van Weerden WM, Oyen WJ and Boerman OC. Imaging of prostate cancer with immuno-PET and immuno-SPECT using a radiolabeled anti-EGP-1 monoclonal antibody. J Nucl Med 2011; 52: 1601-7.

[21] Verel I, Visser GW, Boellaard R, Boerman OC, van Eerd J, Snow GB, Lammertsma AA and van Dongen GA. Quantitative 89Zr immuno-PET for in vivo scouting of 90Y-labeled monoclonal antibodies in xenograft-bearing nude mice. J Nucl Med 2003; 44: 1663-70.

[22] Brouwers A, Verel I, Van Eerd J, Visser G, Steffens M, Oosterwijk E, Corstens F, Oyen W, Van Dongen G and Boerman O. PET radioimmunoscintigraphy of renal cell cancer using 89Zr-labeled cG250 monoclonal antibody in nude rats. Cancer Biother Radiopharm 2004; 19: 155-63.

[23] Perk LR, Stigter-van Walsum M, Visser GW, Kloet RW, Vosjan MJ, Leemans CR, Giaccone G, Albano R, Comoglio PM and van Dongen GA. Quantitative PET imaging of Met-expressing human cancer xenografts with 89Zr-labelled monoclonal antibody DN30. Eur J Nucl Med Mol Imaging 2008; 35: 1857-1867.

[24] Hoeben BA, Kaanders JH, Franssen GM, Troost EG, Rijken PF, Oosterwijk E, van Dongen GA, Oyen WJ, Boerman OC and Bussink J. PET of hypoxia with 89Zr-labeled cG250-F(ab')2 in head and neck tumors. J Nucl Med 2010; 51: 1076-83.

[25] Heuveling DA, Visser GW, Baclayon M, Roos WH, Wuite GJ, Hoekstra OS, Leemans CR, de Bree R and van Dongen GA. 89Zr-nanocolloidal albumin-based PET/CT lymphoscintigraphy for sentinel node detection in head and neck cancer: preclinical results. J Nucl Med 2011; 52: 1580-4.

[26] Nayak TK, Garmestani K, Milenic DE and Brechbiel MW. PET and MRI of metastatic peritoneal and pulmonary colorectal cancer in mice with human epidermal growth factor receptor 1-targeted 89Zr-labeled panitumumab. J Nucl Med 2012; 53: 113-120.

[27] Keliher EJ, Yoo J, Nahrendorf M, Lewis JS, Marinelli B, Newton A, Pittet MJ and Weissleder R. 89Zr-labeled dextran nanoparticles allow in vivo macrophage imaging. Bioconjugate Chemistry 2011; 22: 2383-2389.

[28] Starmans LWE, Hummelink MAPM, Rossin R, Kneepkens ECM, Lamerichs R, Donato K, Nicolay K and Grüll H. 89 Zr- and Fe-Labeled Polymeric Micelles for Dual Modality PET and T1 -Weighted MR Imaging. Adv Healthc Mater 2015; 4: 2137-2145.

[29] Constantinescu CC and Mukherjee J. Performance evaluation of an Inveon PET preclinical scanner. Phys Med Biol 2009; 54: 2885-2899.

[30] Vosjan MJ, Perk LR, Visser GW, Budde M, Jurek P, Kiefer GE and van Dongen GA. Conjugation and radiolabeling of monoclonal antibodies with zirconium-89 for PET imaging using the bifunctional chelate p-isothiocyanatobenzyl-desferrioxamine. Nat Protoc 2010; 5: 739-743.

[31] Hu MC, Shi M, Zhang J, Addo T, Cho HJ, Barker SL, Ravikumar P, Gillings N, Bian A, Sidhu SS,

Kuro-o M and Moe OW. Renal Production, Uptake, and Handling of Circulating αKlotho. J Am Soc Nephrol 2016; 27: 79-90.

[32] Abou DS, Ku T and Smith-Jones PM. In vivo biodistribution and accumulation of ^{89}Zr in mice. Nucl Med Biol 2011; 38: 675-681.

[33] Gkentzi D, Efthymiadou A, Kritikou D and Chrysis D. Fibroblast growth factor 23 and Klotho serum levels in healthy children. Bone 2014; 66: 8-14.

[34] Semba RD, Moghekar AR, Hu J, Sun K, Turner R, Ferrucci L and O'Brien R. Klotho in the cerebrospinal fluid of adults with and without Alzheimer's disease. Neurosci Lett 2014; 558: 37-40.